energies

MDPI

Article

Design of a 1 MW_{th} Pilot Plant for Chemical Looping Gasification of Biogenic Residues

Falko Marx *, Paul Dieringer, Jochen Ströhle and Bernd Epple

Institute for Energy Systems & Technology, Technische Universität Darmstadt, Otto-Berndt-Str. 2, 64287 Darmstadt, Germany; paul.dieringer@est.tu-darmstadt.de (P.D.); jochen.stroehle@est.tu-darmstadt.de (J.S.); bernd.epple@est.tu-darmstadt.de (B.E.)

* Correspondence: falko.marx@est.tu-darmstadt.de; Tel.: +49-6151-16-23002

Abstract: Chemical looping gasification (CLG) is a promising process for the thermochemical solid to liquid conversion route using lattice oxygen, provided by a solid oxygen carrier material, to produce a nitrogen free synthesis gas. Recent advances in lab-scale experiments show that CLG with biomass has the possibility to produce a carbon neutral synthesis gas. However, all experiments have been conducted in externally heated units, not enabling autothermal operation. In this study, the modification of an existing pilot plant for demonstrating autothermal operation of CLG is described. Energy and mass balances are calculated using a validated chemical looping combustion process model extended for biomass gasification. Based on six operational cases, adaptations of the pilot plant are designed and changes discussed. A reactor configuration using two circulating fluidized bed reactors with internal solid circulation in the air reactor is proposed and a suitable operating strategy devised. The resulting experimental unit enables a reasonable range of operational parameters within restrictions imposed from autothermal operation.

Keywords: chemical looping; biomass; gasification; fluidized bed; autothermal; pilot plant

Citation: Marx, F.; Dieringer, P.; Ströhle, J.; Epple, B. Design of a 1 MW_{th} Pilot Plant for Chemical Looping Gasification of Biogenic Residues. *Energies* **2021**, *14*, 2581. https://doi.org/10.3390/en14092581

Academic Editor: Andrea Di Carlo

Received: 31 March 2021
Accepted: 28 April 2021
Published: 30 April 2021

1. Introduction

The reduction of greenhouse gas emissions is one of the major challenges in the 21th century. The European Commission sets a minimum share of 14% as a goal for renewable transport fuels produced from non food or feed sources in 2030 [1] in order to combat global warming according to the UNFCCC Paris Agreement. This is a major increase from the less than 0.1% share of renewable transport fuels in 2018 in the European Union (including food grade sources) [2] and necessitates the development of second generation biofuels. Moreover, first generation biofuels mostly utilize biochemical conversion from sugar and starch or physicochemical conversion from plant oil or fat for the production of drop in fuels [3]. However, these processes cannot be used efficiently for the production of second generation biofuels from EU approved biogenic sources—as they are low in sugar, starch, oil and fat and high in cellulosis and lignin—so new production processes are needed.

However, efficient technological pathways for the production of second generation exist only partially and not in an entire process chain, in the form of thermochemical conversion through gasification, methanol or Fischer–Tropsch synthesis and subsequent refining. Gasification, the starting point of the process chain for solid to liquid conversion, is presently used for the generation of heat and electricity [4] and very little for the production of liquid biofuels [5]. It is a well known process which converts solid feedstock in to a high caloric syngas and is considered to have a high potential for the decarbonization of hard to electrify aviation and maritime transport sectors. Additionally, the energy required for the conversion is provided by the biomass feedstock giving the potential of a total carbon neutral drop-in fuel.

As the feedstocks considered by the European Union [1] include seasonally varying types of biomass like husk and straw, as well as more continually sourceable foresting residue, sewage sludge, and biogenic household waste, fluidized bed gasification with its good feedstock flexibility seems a suitable process. Moreover, the good heat and mass transfer characteristics of fluidized bed facilitate complete conversion of the feedstock into syngas, thus achieving a high carbon conversion [6,7] and process efficiency [7,8]. Furthermore, as fuel synthesis requires an N_2-free syngas and thus gasification without the presence of N_2 [9], the subsequent syngas cleaning gives rise to easy carbon capture with storage or utilization making the carbon footprint of the product negative. The N_2-free gasification environment is usually created by the provision of pure oxygen provided by an air separation unit (ASU) [9,10], but in fluidized bed gasification another possibility exists to create an N_2-free atmosphere: dual fluidized bed gasification (DFBG) utilizes two reactors to split the gasification process from the oxidation or combustion process used to generate the necessary heat while avoiding the expensive ASU. Nonetheless, as heated solid bed material circulating between the two reactors is used to transfer the energy for the process, the transport of some amounts of carbon from the feedstock to the gasification reactor is necessary for the combustion reactor to generate the required heat, giving a substantial amount of CO_2-emission from the process.

The chemical looping gasification (CLG) process operates in a similar manner using two coupled fluidized bed reactors. However, instead of transporting residual feedstock from the gasification reactor to one operated with air, it employs a metal oxide to transport oxygen from a reactor operated with air towards the gasification, thus giving the benefit of a process with virtually no CO_2 emission. So far all experiments with continuous operation of the process were conducted in lab and pilot scale with external heating [11–15] and a maximum thermal load of 25 kW [16,17]. Furthermore, autothermal operation has not been demonstrated and problems of process scale up have not been identified and alleviated. Therefore the existing 1 MW chemical looping combustion (CLC) pilot plant located at Technische Universität Darmstadt is modified for the operation and investigation of the CLG process with biomass.

In this work, the design and modifications of the 1 MW pilot plant are described. Starting from the underlying, fundamental gasification process, the existing infrastructural restrictions, and the planed operation range, mass and energy balances are calculated and required adjustments identified and implemented.

2. Theory

2.1. Gasification Fundamentals

Fluidized bed CLG of solid feedstocks comprises, after initial drying and devolatilization, the following main reactions:

$$C + CO_2 \longleftrightarrow 2\,CO \qquad \Delta H = 172.4\,\mathrm{kJ\,mol^{-1}} \qquad \text{Bodouard reaction} \qquad \text{(R1)}$$

$$C + H_2O \longleftrightarrow CO + H_2 \qquad \Delta H = 131.3\,\mathrm{kJ\,mol^{-1}} \qquad \text{char reforming} \qquad \text{(R2)}$$

$$CO + H_2O \longleftrightarrow CO_2 + H_2 \qquad \Delta H = -41.1\,\mathrm{kJ\,mol^{-1}} \qquad \text{water gas shift} \qquad \text{(R3)}$$

$$C + 2\,H_2 \longleftrightarrow CH_4 \qquad \Delta H = -74.8\,\mathrm{kJ\,mol^{-1}} \qquad \text{methanation} \qquad \text{(R4)}$$

Further important reactions between the commonly used gasification agent H_2O [9] and the formed methane is the steam methane reforming reaction:

$$CH_4 + H_2O \longleftrightarrow CO + 3\,H_2 \qquad \Delta H = 206.1\,\mathrm{kJ\,mol^{-1}} \qquad \text{steam methane reforming} \qquad \text{(R5)}$$

$$CH_4 + 2\,H_2O \longleftrightarrow CO_2 + 4\,H_2 \qquad \Delta H = 165\,\mathrm{kJ\,mol^{-1}} \qquad \text{steam methane reforming} \qquad \text{(R6)}$$

where reaction (R6) is the combination of reactions (R3) and (R5).

The influence of reactions (R5) and (R6) largely depends on the formed methane from devolatilization and reaction (R4). These reactions require a high amount of heat, as indicated by the reaction enthalpies, thus greatly contributing to the overall endothermic re-

action inside the fuel reactor (FR). Moreover, it is clear that higher gasification temperatures lead to lower amounts of CH_4.

Reactions (R1) and (R2) necessitate a high amount of heat which cannot be balanced by the exothermic reactions (R3) and (R4) and has to be supplied for the gasification process. This heat can either be provided in situ through the oxidation of part of the feedstock (syngas species, volatiles and char) or externally e.g., through supply of a bed material heated in a second reactor enabling an autothermal process. The CLG process, schematically shown in Figure 1, employs both routes to supply the gasification energy. The solid oxygen carrier (OC) material supplies sensible heat to the fuel reactor (FR) while also providing lattice oxygen for the oxidation of part of the feedstock.

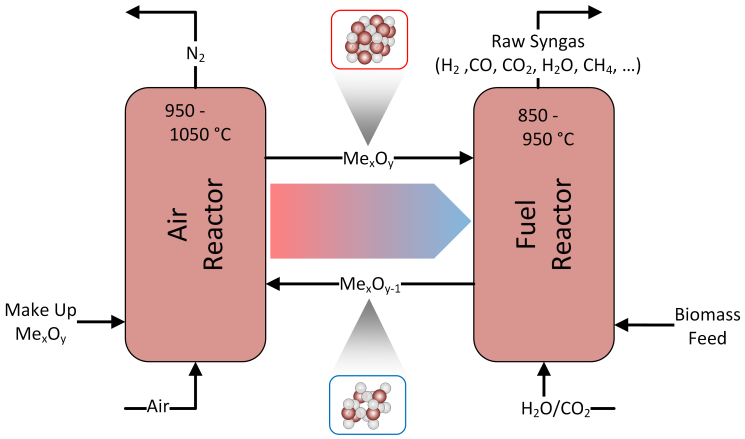

Figure 1. Schematic of the CLG process showing the cyclic reduction and oxidation of an OC material which is oxidized in the air reactor (AR) and reduced in the fuel reactor (FR).

However, additional reactions have to be considered when the bed material is a chemically active part of the feedstock conversion. In the FR where the OC material is reduced the reactions are:

$$\mathrm{Me}_x\,\mathrm{O}_y + \mathrm{CH_4} \longrightarrow \mathrm{Me}_x\mathrm{O}_{y-1} + 2\,\mathrm{H_2} + \mathrm{CO} \quad \text{(R7)}$$

$$4\,\mathrm{Me}_x\,\mathrm{O}_y + \mathrm{CH_4} \longrightarrow 4\,\mathrm{Me}_x\mathrm{O}_{y-1} + 2\,\mathrm{H_2O} + \mathrm{CO_2} \quad \text{(R8)}$$

$$\mathrm{Me}_x\,\mathrm{O}_y + \mathrm{CO} \longrightarrow \mathrm{Me}_x\mathrm{O}_{y-1} + \mathrm{CO_2} \quad \text{(R9)}$$

$$\mathrm{Me}_x\,\mathrm{O}_y + \mathrm{H_2} \longrightarrow \mathrm{Me}_x\mathrm{O}_{y-1} + \mathrm{H_2O} \quad \text{(R10)}$$

$$m\,\mathrm{Me}_x\,\mathrm{O}_y + \mathrm{C}_m\,\mathrm{H}_n \longrightarrow m\,\mathrm{Me}_x\,\mathrm{O}_{y-1} + \mathrm{mCO} + \mathrm{n}/2\,\mathrm{H_2O} \quad \text{(R11)}$$

$$2\,\mathrm{Me}_x\,\mathrm{O}_y + \mathrm{C} \longrightarrow 2\,\mathrm{Me}_x\,\mathrm{O}_{y-1} + \mathrm{CO_2} \quad \text{(R12)}$$

Solid–solid reactions between char and OC (R12) are generally slower than the heterogeneous gas solid reactions (R7) to (R10) and can therefore be neglected [18,19] except for very high reaction temperatures [20]. The reduced OC is then transported to the air reactor (AR), where it is oxidized with air in an exothermic reaction:

$$\mathrm{Me}_x\,\mathrm{O}_{y-1} + 0.5\,\mathrm{O_2} \longrightarrow \mathrm{Me}_x\mathrm{O}_y \quad \text{(R13)}$$

$$\mathrm{C} + \mathrm{O_2} \longrightarrow \mathrm{CO_2} \quad \text{(R14)}$$

Inside the AR the combustion of char, reaction (R14) is favored above the oxidation of OC through reaction (R13) [20–22], so residual char transported with the OC from the FR to the AR will be combusted before the oxidation of the OC, adding to the full feedstock conversion and supplying additional heat to the exothermic re-oxidation, (R13). However, (R14) is undesired during CLG, as it reduces the major advantage of a virtually CO_2-free flue gas stream from the AR when compared to DFBG.

CLG has been demonstrated to work as a continuous process in externally heated bench and lab-scale units up to 25 kW [17]. Large-scale experiments at Chalmers

University [23] suffer from the necessity of the AR to supply hot water for building heating and thus the requirement of significant fuel feeding to the AR. Therefore, exhibiting a severe mismatch of reactor dimension of factor 3 to 6 [24] while not depending on (R13) for heat release inside the AR. Hence, these experiments cannot be considered autothermal or even CLG, creating a need for experiments in a bigger scale to confirm the possibility and investigate the performance of autothermal CLG.

Process parameters considered important during the design are the cold gas efficiency:

$$\eta_{CG} = \frac{\dot{n}_{FR,out}(X_{\mathrm{CH_4}} \cdot LHV_{\mathrm{CH_4}} + X_{\mathrm{CO}} \cdot LHV_{\mathrm{CO}} + X_{\mathrm{H_2}} \cdot LHV_{\mathrm{H_2}})}{\dot{m}_{FS} \cdot LHV_{FS}} \quad (1)$$

with X_i being the mole fraction of species i, LHV the lower heating value, and $\dot{n}_{FR,out}$ and $\dot{m}_{FS}$ being the product gas output and the feedstock input, respectively. The oxygen carrier to fuel equivalence ratio is defined by [25]:

$$\phi = \frac{R_{OC} \cdot \dot{m}_{OC} \cdot X_{s,AR}}{\dot{m}_{O,stoich}} \quad (2)$$

$$X_{s,AR} = \frac{m_{OC,AR} - m_{OC,red}}{R_{OC} \cdot m_{OC,ox}} \quad (3)$$

In this definition the oxygen required for full feedstock conversion is $m_{O,stoich}$, R_{OC} is the oxygen transport capacity of the OC material, $X_{s,AR}$ is the oxidation degree of the OC, $m_{OC,red}$ and $m_{OC,ox}$ are the mass of the fully reduced and oxidized state respectively, while the mass of the OC leaving the AR is $m_{OC,AR}$. For gasification ϕ has to be smaller than unity to prevent the full oxidation of the feedstock [25,26]. However, syngas formation is observed even for values of $\phi > 1$ [27]. Values of $\phi < 1$ can be achieved by reducing the mass flow $\dot{m}_{OC}$ or the OC oxidation, i.e., $m_{OC,AR} - m_{OC,red}$. The first option has the disadvantage of also influencing the heat transport $\dot{Q}$ between the reactors:

$$\dot{Q} = \dot{m}_{OC} \cdot c_p \cdot \Delta T \quad (4)$$

with c_p, the heat capacity of the OC and ΔT, the temperature difference of OC particles entering and leaving the FR. The influence of the OC oxidation on c_p is small and can be compensated by adjustments of $\dot{m}_{OC}$ during practical application of option two.

Additionally the fraction of syngas in the dry product gas is defined as:

$$x_{SG} = \frac{X_{\mathrm{CO}} + X_{\mathrm{H_2}}}{X_{\mathrm{CH_4}} + X_{\mathrm{CO}} + X_{\mathrm{H_2}} + X_{\mathrm{CO_2}} + X_{\mathrm{H_2S}} + X_{\mathrm{N_2}}} \quad (5)$$

2.2. Bed Materials for Chemical Looping Gasification

The selection and testing of bed materials is a crucial task when designing a CLG process. Eight criteria for CLC are given by Adanez et al. [28] and repeated here with notes on how they apply to CLG:

1. Oxygen transport capacity: as gasification processes limit the supply of oxygen below the stoichiometric ratio required for full feedstock conversion, a high oxygen transport capacity is not so important as the process is limited by the sensible heat transported and not the oxygen [16,26]. For CLC the supply of excess oxygen is not critical, for CLG it must be limited without impairing the transport of sensible heat as otherwise, the temperature in the FR would drop, negatively influencing the gasification [26].
2. Thermodynamic suitability: the bed material must be able to oxidise the feedstock at least partially while not releasing molecular oxygen. Thus chemical looping with oxygen uncoupling (CLOU) materials cannot be used for CLG.
3. High reactivity over multiple reduction-oxidation cycles: activation over multiple cycles can increase or decrease reactivity.

4. Stability: the expected lifetime of the bed material should be as long as possible, as losses through attrition need to be compensated by a make-up stream. This make-up stream requires heating to process temperature, thus always leading to an efficiency drop. Measurement and calculation of OC lifetime is not straightforward and can vary by a factor of 3.2 for one experiment depending on the method used [29].
5. Carbon deposition: carbon transport towards the AR with subsequent combustion negatively impacts carbon utilization and capture efficiency. However, Adanez et al. [28] note that no carbon deposition has been found in relevant studies.
6. Fluidization properties: formation of agglomerates or low melting compounds with parts of the feedstock must be avoided. This becomes difficult if a herbaceous feedstock—high in ash and alkali metals—is used and might require mitigation measures like pre-treatment [30,31] or feedstock mixing [32].
7. Cost: the current production cost for synthetic materials make them non competitive when compared to naturally occurring minerals or waste materials.
8. Toxicity: deployment of environmental friendly and non-toxic OC material avoids special and costly requirements during handling and disposal of deactivated OC material.

Moreover, the design for pilot and demonstration plants need to consider an additional point:

9. Availability: the selected material must be available in the required quantity. Synthesized OC materials are not available on a commercial scale yet. So a natural ore or a waste material must be used.

Especially OC materials which are categorized as materials for syngas production [33–35] are problematic as they are either synthetic materials not available in the required quantities, expensive or toxic to humans and the environment. However, even materials with full oxidization capability for combustion can be used for the production of high calorific syngas when suitable control concepts are employed [11,16,26]. While lots of operating experience with bed materials for DFBG in the range above 1 MW exists [36], there is little experience with OC materials in the same power range [23,25]. However, even those experiments do not give a good indication of their process performance, as the AR—or rather combustor, as it is always fed with fuel—used is oversized by a factor of 3 to 6 [24], effectively creating a reservoir of OC and sensible heat more dependent on the required energy for heating supply than the CLG process. Moreover, higher attrition rates of e.g., ilmenite are reported for CLG when compared with CLC [11] but if the effects are the same in a bigger CLG plant is still an open question. Due to the small size of lab-scale reactors, the OC material undergoes more oxidation/reduction cycles per hour, thus giving higher stress from chemical conversion when compared to the mechanical stress from the transport through the reactors and coupling elements.

Depending on the requirements of the targeted application for the syngas, a last point is to be considered when selecting the OC bed material:

10. Catalytic properties: selecting a material (or additive) which catalytically reduces the formation of unwanted components like tars [37,38] and CH_4 [39] or binds elements to the solid fraction (e.g., sulphur in form of gypsum) as a primary method. Secondary gas cleaning methods might therefore not be necessary or can be designed much smaller.

Tar production is of major concern for subsequent syngas treatment especially for biomass gasification where tar production is high [40]. Bed height, bed material, temperatures, velocities, feedstock, and feedstock feeding location [37] have an influence on the production of tars. Existing kinetic models for the prediction of tar production are not applicable as they are developed for a very specific process and reactor size [15], need fitting against the actual reactor performance [41], or are not reliable in the prediction of tars formed [42–44]. Furthermore, no model was developed for CLG yet.

3. Process Design

In the following, the CLG technology fundamentals described in Section 2 are combined with boundary conditions from the existing pilot plant as well as feedstock properties and hydrodynamic characteristics yielding a process design suitable for the demonstration of autothermal CLG in the existing 1 MW_{th} pilot plant.

3.1. Existing Pilot Plant

The heart of the CLG pilot plant consists of two refractory lined circulating fluidized bed (CFB) reactors which are coupled using two loop seals and one J-valve and have properties indicated in Table 1. The CFB400-reactor of the pilot plant has been used as gasifier for High Temperature Winkler (HTW^{TM}) gasification [45,46] and as FR in the CLG-related processes for chemical looping combustion, while the CFB600-reactor has been used as AR [47–51]. Thus major components can be reused for CLG by combining elements from the CLC and the HTW^{TM} process configurations. Nonetheless, major adaptations are made, as the HTW^{TM} configuration is build for lower fluidization velocities and with 0.5 MW_{th} [45] also for lower thermal input.

Table 1. Reactor properties of the 1 MW CLG pilot plant.

Reactor	AR—CFB600	FR—CFB400	Unit
Height	8.66	11.35	m
Inner diameter	0.59	0.28 to 0.4	m
Outer diameter	1.3	1.0	m
Temperature	1050	950	°C
Fuel feeding	in bed (propane lance), return leg of LS 4.5 (solids)	in bed via screw (solids)	

Furthermore, as electrical preheating temperatures of fluidization media are limited to 400 °C, process stream heating has to be done inside the reactors, negatively impacting cold gas efficiency which would be optimized in an industrial plant using heat integration. The cooling system sets a limit of 1 MW_{th} which can be safely handled for CLC. However, as a major part of the energy of the feedstock remains as heating value in the product gas, feedstock input above the 1 MW_{th} is possible for CLG.

Therefore the following case has been set as design specifications for the investigations of CLG for which mass and energy balances were calculated, required changes to the pilot plant identified and modifications designed.

- As the cooling system is designed to handle a thermal load of 1 MW safely, the design power of the pilot plant is is set to 1 MW_{th}.
- Ilmenite as OC: For the selected thermal power, a total inventory of about 1000 kg was used during CLC experiments in the pilot plant [50], and the same can be expected for CLG. Thus, of the points listed in Section 2.2, the availability is a major concern for experiments in that scale, and a natural ore or a widely available waste material had to be selected. Recent studies show promising results for ilmenite in continuous units [11], and operating experience with ilmenite in the pilot plant exists [49,50]. Moreover, ilmenite has been shown to catalytically reduce tars [25,52].
- Temperatures for the AR of 1050 °C and 950 °C are considered the maximum viable temperatures. Higher FR temperatures will yield a higher H_2/CO ratio at the expense of lower cold gas efficiency. So slightly lower FR temperatures might be desired in industrial application. Moreover, as OC ash interaction may lead to problems at high temperatures [31] and the temperature difference between the reactors is an important parameter for process control [26], the FR temperature is not fixed and considered an important variable in the planned experiments.
- Industrial wood pellets as feedstock as described in Section 3.2.

3.2. Feedstocks

As model feedstock for the calculation of the heat and mass balances and the design of modifications, industrial wood pellets have been selected, as they are widely available and allow for easy comparison with existing gasification technologies in pilot and demonstration scale where wood based materials are gasified [36]. Additionally, wheat straw, as a seasonal varying biomass source, and pine forest residue, as a more constant source, are selected as feedstocks from the EU-approved list [1] for experimental investigations.

Initial investigations of wheat straw by Di Giuliano et al. [31] indicate that it is a difficult feedstock for CLG, due to its low ash softening point and the possibility to cause agglomerates and bed defluidization, so that it requires at least some pre-treatment. However, as fluidization velocities in the CFB reactors are two magnitudes higher than the investigated fluidization velocities, the required pre-treatment cannot be directly inferred, but a higher fluidization velocity seems to lower the required pre-treatment effort [31]. Moreover, reaction kinetics for pelletized wheat straw in various bed materials are similar to pellets of pine forest residue [53] opening up possibilities to switch between these feedstocks during gasifier operation. Nevertheless, additional investigations on the pre-treatment of wheat straw are needed to be able to give accurate information on the fuel properties—which are indicated in Table 2 for the planed feedstocks—as they vary with pre-treatment. It is assumed that pre-treatment of wheat straw will make handling and gasification easier, as it reduces agglomeration tendencies (additivation, torrefaction) and water content (drying, torrefaction). Thus, raw wheat straw is the most difficult to gasify and can be used as a lower end in feedstock quality.

Table 2. Proximate and ultimate analysis of feedstocks.

	Component	Wood Pellets	Pine Forest Residue	Wheat Straw
Proximate Analysis in wt. − %	Moisture	6.5	7	7
	Ash (d.b.)	0.7	1.86	7.5
	Volatiles (d.b.)	85.1	78.86	81.5
	Fixed carbon (d.b.)	14.2	12.28	11
Ultimate Analysis in wt. − %	C (d.a.f.)	50.8	52.7	48.2
	H (d.a.f.)	6	6.4	6.5
	N (d.a.f.)	0.07	0.39	0.43
	O (d.a.f.)	43.2	40.5	44.9
	S (d.a.f.)	0.008	0.05	0.11
	Cl (d.a.f.)	0.006	0.007	0.05
Net calorific value in MJ kg^{-1}		17.96	18.41	17.12

3.3. Heat and Mass Balances

Heat and mass balances for the pilot plant were calculated considering reaction kinetics of ilmenite and reactor hydrodynamics using a validated Aspen Plus™ model for CLC [51] extended to cover biomass gasification via a Langmuir–Hinschelwood mechanism [26]. However, instead of an equilibrium model used by Dieringer et al. [26], the more realistic original reaction kinetics for ilmenite were used for the OC gas reaction. As a starting point, the CLC case was selected in terms of reactor dimensions, temperatures, solid inventories, pressure, and loop seal (LS) fluidization. The feedstock flow $\dot{m}_{FS}$ (industrial wood pellets) was selected as 1 MW_{th}, and the heat losses were assumed to be 110 kW which falls in the reported range of 60 kW to 200 kW [48,50]. Furthermore, heat losses are considered to be dependent on reactor temperature and independent of feedstock input. LS fluidization with CO_2 is set to 84.2 kg h^{-1} based on previous operating experience [49,50]. To obtain autothermal operation at these conditions, the oxygen availability inside the AR was varied through the inlet feed rate of air into the AR, while the heat transport between both reactors was controlled through the global metal oxide solid circulation rate ($\dot{m}_{OC,AR,out}$, $\dot{m}_{OC,FR,out}$), until both reactors were in heat balance. The hydrodynamic constraints related

to the required solid entrainment (calculated as suggested by Kunii and Levenspiel [54], described in detail elsewhere [51,55]) from each reactor were achieved by varying the steam inlet flow $\dot{m}_{H_2O}$ and flue gas recirculation inlet flow $\dot{m}_{AR,reci}$ for the FR and AR, respectively, while setting internal solid circulation to zero. All boundary conditions are listed in Table 3, and the corresponding results are in Table 4. The listed streams are visualized in the reactor configuration in Figure 2.

Table 3. Boundary conditions for the simulation of autothermal CLG operations of the 1 MW pilot plant.

Property	Value	Unit	Property	Value	Unit
$d_{p,50}$	154	µm	$T_{Gas,in}$	400	°C
Δp_{FR}	61	mbar	Δp_{AR}	90	mbar
p_{FR}	1	bar	p_{AR}	1	bar
d_{FR}	0.28 to 0.4	m	d_{AR}	0.59	m
h_{FR}	11.35	m	h_{AR}	8.66	m

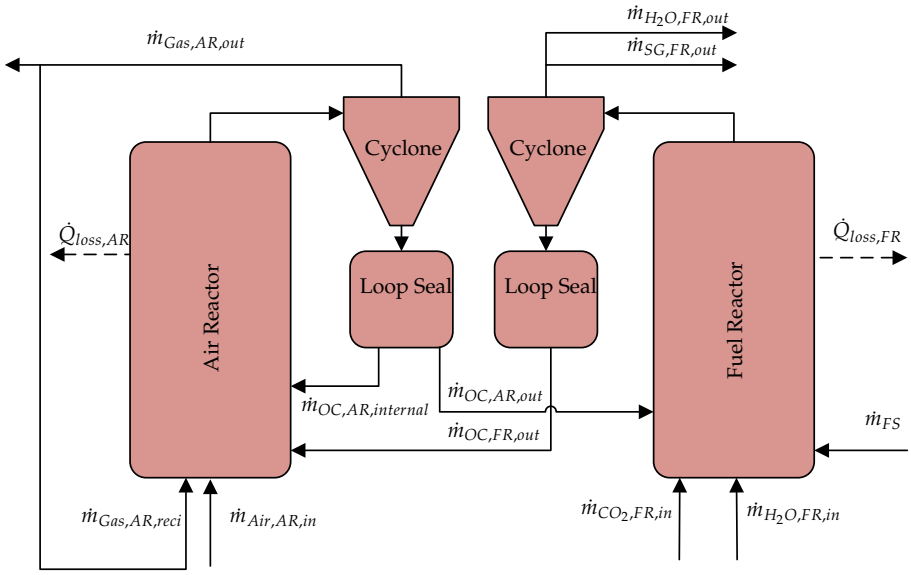

Figure 2. Streams for the calculation of mass and energy balances of the CLG process.

In small scale units where the energy is supplied via furnace heating, the oxygen supply can be controlled via the circulation. However, in the 1 MW pilot plant the heat is supplied only via the circulation of the bed material. From the results of the Reference case, it can be seen that the transport of oxygen must be limited in order to obtain a good gasification process, while the solid circulation must remain high as indicated by the substantial amount of recirculated gas fed to the reactor. Thus, a new control method for the oxygen transport must be realised, decoupling the transport of oxygen from the transport of sensible heat as described by Dieringer et al. [26]. Moreover, the superficial gas velocity u_0 in the AR is below the range of a CFB, as shown in Figure 3, while the calculated solid flux G_S is also below the range commonly observed in commercial CFB units [56]. Indeed, past operation of the AR showed good performance with superficial gas velocities of approximately 3.5 m s^{-1} to 5 m s^{-1}. In the pilot plant, the installation of a (partial) flue gas recirculation for the AR is used to increase u_0 while also supplying the inert fluidization medium required for the process control. Increasing the solids discharge from the AR—while keeping the global solids circulation constant—creates the need for an internal solid circulation in the AR—where material not transported through the J-valve is returned via the LS—which is not common in smaller units. In fact, most lab- and bench-scale units have internal solids recirculation for the FR to enhance carbon conversion [57] or no solids

recirculation at all [11,17]. Nonetheless, this solution comes with a penalty, as additional fluidization medium is needed and has to be heated to process temperature. However, reducing the diameter of an existing, refractory lined reactor is costly and time consuming, so the efficiency penalty has to be accepted; yet it also opens the possibility to use the start-up burner for fast temperature adjustments in-between experimental set points without severe impact on reactor hydrodynamics. In a commercial unit, the diameter would be designed according to process specification and corresponding hydrodynamics, requiring the flue gas recirculation only for process control. Nonetheless, this initial estimation shows that CLG is possible in the existing 1 MW pilot plant.

Table 4. Simulation results for autothermal CLG operations of the 1 MW pilot plant. Stream names correspod to Figure 2. Boundary conditions deviating from the reference case are underlined. The first block contains the thermodynamic and hydrodynamic constraints and results, the second block contains the process streams (in some cases with composition). The third block gives information on solid composition for the FR, while the last block shows general process performance parameters.

Stream	Reference	HT1	HT2	HF	HP1	HP2	Unit
T_{AR}	1025	1050	1050	1025	1025	1025	°C
T_{FR}	900	900	950	900	900	900	°C
$\dot{m}_{FS}$	200.4	200.4	200.4	200.4	240.48	280.56	kg h^{-1}
$u_{0,AR}$	3.42	3.12	3.97	5.03	5.01	5.01	m s^{-1}
$u_{0,FR}$	6.25	5.46	7.64	5.67	6.23	6.75	m s^{-1}
$\dot{Q}_{loss,AR}$	48.5	49.4	49.9	49.3	50.5	49.6	kW
$\dot{Q}_{loss,FR}$	59.8	61.8	59.8	61.3	59.4	61.2	kW
$\dot{m}_{OC,AR,out}$	7180	5690	9979	6244	7257	8285	kg h^{-1}
$\dot{m}_{OC,FR,out}$	7130	5649	9906	6175	7199	8236	kg h^{-1}
$\dot{m}_{OC,AR,internal}$	0	0	0	12,120	10,994	9971	kg h^{-1}
$\dot{m}_{Air,AR,in}$	640	600	745	730	760	802	kg h^{-1}
$\dot{m}_{Gas,AR,out}$	950.6	854.6	1062.7	1404.3	1413.6	1425.5	kg h^{-1}
— $X_{CO_2,AR}$	0.111	0.117	0.096	0.098	0.111	0.122	
— $X_{O_2,AR}$	0.004	0.003	0.005	0.005	0.004	0.003	
$\dot{m}_{AR,reci}$	360.7	296.3	391.2	744.3	708.2	672.8	kg h^{-1}
$\dot{m}_{H_2O,FR,in}$	301.53	237.04	383.83	247.14	263.4	276.94	kg h^{-1}
$\dot{m}_{CO_2,FR,in}$	84.2	84.2	84.2	84.2	84.2	84.2	kg h^{-1}
$\dot{m}_{H_2O,FR,out}$	362.9	294.5	451.5	318.8	337.9	354.0	kg h^{-1}
$\dot{m}_{Syngas,FR,out}$	271.1	267.0	287.8	280.5	307.3	334.3	kg h^{-1}
— $X_{CO_2,FR}$	0.466	0.439	0.543	0.531	0.440	0.377	
— $X_{CO,FR}$	0.304	0.317	0.240	0.277	0.324	0.354	
— $X_{CH_4,FR}$	0.092	0.099	0.057	0.072	0.095	0.113	
— $X_{H_2,FR}$	0.139	0.145	0.160	0.119	0.141	0.156	
— $X_{H_2S,FR}$	5.26×10^{-5}	5.22×10^{-5}	5.13×10^{-5}	5.38×10^{-5}	5.48×10^{-5}	5.56×10^{-5}	
$\dot{n}_{Solid,FR,out}$	14.84	11.54	20.60	13.38	15.09	16.90	mol h^{-1}
— $X_{C,out}$	0.04	0.05	0.03	0.05	0.05	0.05	
— $X_{Fe_2O_3,out}$	0.09	0.06	0.10	0.13	0.09	0.07	
— $X_{FeTiO_3,out}$	0.68	0.76	0.66	0.57	0.68	0.74	
— $X_{TiO_2,out}$	0.18	0.12	0.21	0.25	0.18	0.14	
$\dot{n}_{Solid,FR,in}$	15.55	12.11	21.70	14.43	15.93	17.54	mol h^{-1}
— $X_{Fe_2O_3,in}$	0.17	0.16	0.18	0.23	0.19	0.15	
— $X_{FeTiO_3,in}$	0.48	0.53	0.47	0.30	0.44	0.55	
— $X_{TiO_2,in}$	0.35	0.31	0.35	0.46	0.37	0.30	
— $X_{Fe_3O_4,in}$	0.00	0.00	0.00	0.00	0.00	0.00	
η_{CG}	0.474	0.505	0.384	0.396	0.475	0.531	
x_{SG}	0.443	0.462	0.400	0.396	0.465	0.511	
ϕ	0.585	0.412	0.836	0.729	0.537	0.412	

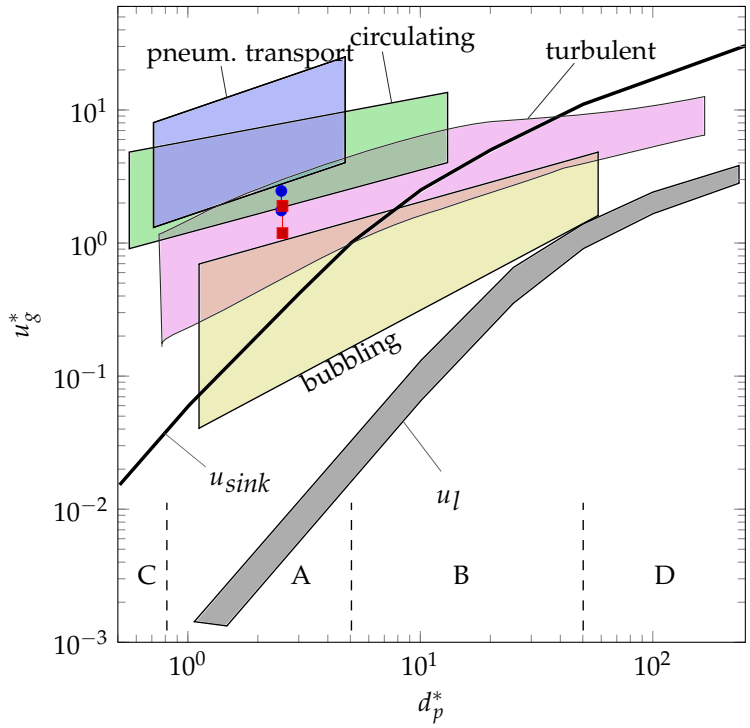

Figure 3. Grace diagram indicating the operation regimes of the FR —●— and AR —■—.

In order to asses the exact limits and to find the corresponding bottle necks where adaptations are needed, some variations on the boundary conditions have been made to be able to decide on equipment alteration and to generate data for the subsequent detailed design. While the simulation of the reference case yields a cold gas efficiency η_{CG} of 0.474, values above 0.8 are reported for externally heated continuous units with a slight increase of η_{CG} with increasing FR temperature [11]. Thus, two additional points with increased AR temperature (HT1) and increase of both reactor temperatures (HT2) were considered to test the feasibility of higher temperatures in the 1 MW pilot plant. The low superficial gas velocity for the AR was raised to $u_{0,AR} = 5\,\mathrm{m\,s^{-1}}$ by increasing the flow of fluidization medium (HF) to see the effect and possibility at higher inlet and outlet streams. This case was also used as a basis for an increase in fuel input to 1.2 MW (HP1) and 1.4 MW (HP2) to reduce the relative impact of heat loss and test the limits of the syngas handling equipment. During experimental operation, the AR superficial velocity would be targeted at slightly above the minimum discharge needed for either stable operation or required by the process—whichever is higher—in order to keep the negative impact of heat demand by fluidization medium low. However, for design purposes, the upper end of the range has to be considered.

From the variation of the reactor temperatures, it is clear that increasing the AR temperature is beneficial to process efficiency, while also increasing the FR, negatively impacts the process performance. For HT1 the increased heating demand in the AR is counteracted by the reduced solids circulation ($\dot{m}_{OC,FR,out}$ and $\dot{m}_{OC,AR,out}$) needed to supply the heat for the gasification process and thus reducing the overall amount of required fluidization medium ($\dot{m}_{Air,AR,in}$, $\dot{m}_{AR,reci}$ and $\dot{m}_{\mathrm{H_2O},FR,in}$) to achieve this lowered solids circulation. The higher FR temperature in HT2 leads to a syngas composition higher in H_2 and lower in CH_4 which is desired, but also requiring significantly higher solids circulation. The corresponding heating requirement of fluidization medium negatively impacts process efficiency. The influence on the syngas quality is caused not only by the raise in gasification temperature, but also in the added steam content from fluidization, influencing reactions (R3), (R5) and (R6). The biggest effect has the increase of the oxygen carrier to fuel equivalence ratio ϕ which raises the relative contribution of oxidation reactions (R8) to (R12).

The increase in AR solids entrainment through higher fluidization velocity (HF) essentially decouples the reactor hydrodynamics of both reactors. Here the model constraint of no internal solids circulation $\dot{m}_{OC,AR,internal}$ is omitted. Instead, the superficial gas velocity $u_{0,AR}$ is targeted at $5\,\mathrm{m\,s^{-1}}$. The higher heat demand for the fluidization medium here has to be supplied by exothermic reaction (R13) leading to a higher degree of OC oxidation as indicated by the increase in ϕ. Consequently, the solids circulation between the reactors is lowered as more oxygen is supplied per OC mass. This leads to lower fluidization requirements and heat demand in the FR reducing the negative impact of the higher fluidization velocity in the AR. Increasing the feedstock input $\dot{m}_{FS}$ while keeping the AR hydrodynamic constant (HP1 and HP2) positively influences process efficiency, as the relative increase in FR fluidization medium required for solids discharge is only about half of the relative increase in feedstock. Thus, only a relatively small part of the additional feedstock is used to cover the energy requirement of the additional fluidization medium, while most of the additional feedstock energy is available for the conversion into syngas making a positive impact on syngas content and cold gas efficiency. This positive influence is mostly caused by more beneficial reactor hydrodynamics and lower relative heat losses of the reactors.

The simulated cases shed light on the process range the reactors can be operated without major modifications, and also highlights the huge impact of heat loss and heat demand in this scale of experiments. It shows that higher FR temperatures in case HT2 require higher fluidization and bigger size of downstream syngas equipment than significant increases in feedstock input (HP2) making this the more critical case to be considered during design. Although the syngas quality increases with higher FR temperature, the cold gas efficiency is drastically reduced, which is in contrast to the observations from Condori et al. [11]. This discrepancy can be explained by the external heating in the lab-scale plant, which can thus compensate the higher heating demands of the process streams. The positive effect of high temperatures for process streams entering the reactors has been shown [26], highlighting the need of good heat recovery and integration for the process. Moreover, the simulated process conditions make clear that individual variations of process parameters like steam to biomass ratio, or oxygen carrier to fuel equivalence ratio ϕ as done by Condori et al. [11] are not possible if no external heating is available. Instead, the CFB mode and the defined solid discharge required for the heat transport also lower the steam to biomass ratio and oxygen carrier to fuel equivalence ratio, as can be seen by the feedstock increase (HP1, HP2). Furthermore, the predicted influence of these combined changes is not necessarily the same as the one observed in small-scale experiments. This can bee seen by the increase of X_{CH_4} with increasing feedstock input, where the accompanying changes in steam to biomass ratio and oxygen carrier to fuel equivalence ratio lead to lower CH_4 in the experiments described by Condori et al. [11].

Confirmation or refutation of either the trends experimentally observed in small scale units or simulated for the existing pilot plant necessitates experiments in the $1\,\mathrm{MW}_{th}$ range where autothermal operation—instead of external electrical heating—becomes necessary. Here, the requirements imposed by autothermal operation of the process limit the range of applicable parameter variation as they are interdependent. Therefore, the existing pilot plant is modified to provide the experimental data needed.

4. Plant Design

The flow sheet in Figure 4 shows a simplified configuration of the designed pilot plant, including major components and important subsystems. Some of the components already available from CLC and HTW^{TM} can be reused, while other subsystems are new or altered. For all subsystems affected by the new CLG process and the alterations a HAZOP analysis has been performed to ensure safe operation.

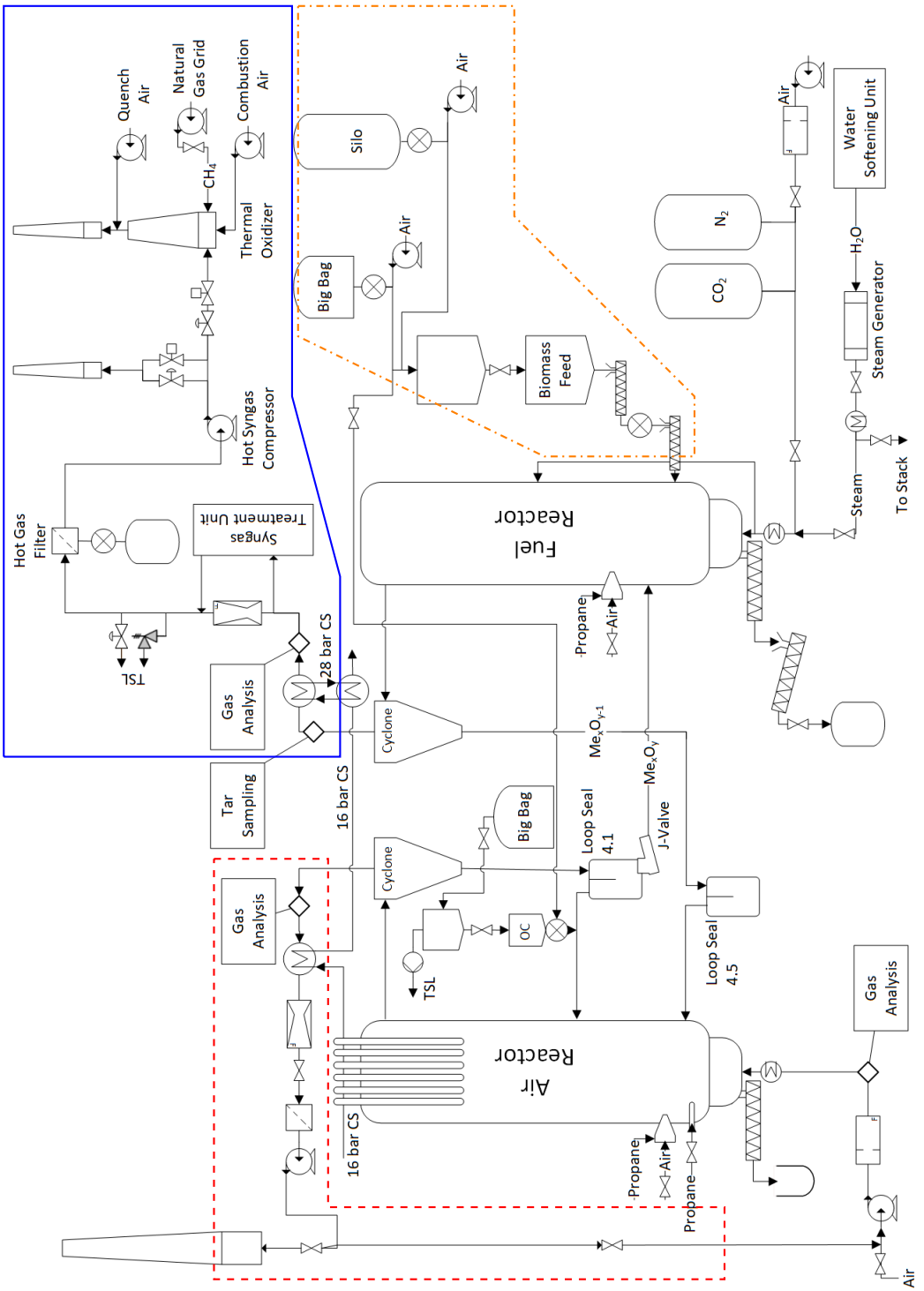

Figure 4. Schematic of the CLG pilot plant showing the main subsystems. CS: cooling system, OC: oxygen carrier, TSL: to safe location. syngas handling: —, flue gas handling: - -, biomass feeding: -·-.

4.1. Reactor System

The reactor system (Figure 5) comprises of the two CFB reactors, two LS and a J-Valve as coupling elements. The total inventory of bed material during CLG operation with ilmenite is about 1000 kg with approximately 250 kg in the AR, 80 kg in the FR, and the rest in the coupling elements. Transport of sensible heat to the FR is not facilitated by internal solid circulation and additional fluidization medium would be required, cooling down the reactor and negatively impacting on process efficiency. Thus, no internal circulation is implemented for the FR. Moreover, process simulations show only reduced OC leaving

the reactor [26] giving no benefit of returning it from the cyclone to the reactor. However, the Gibbs reactor model employed in this study leads to full conversion, while in reality a mixture of different phases will always be present. Nonetheless, the prevalence of highly reduced phases in both FR and AR has been confirmed in continuous experiments [11].

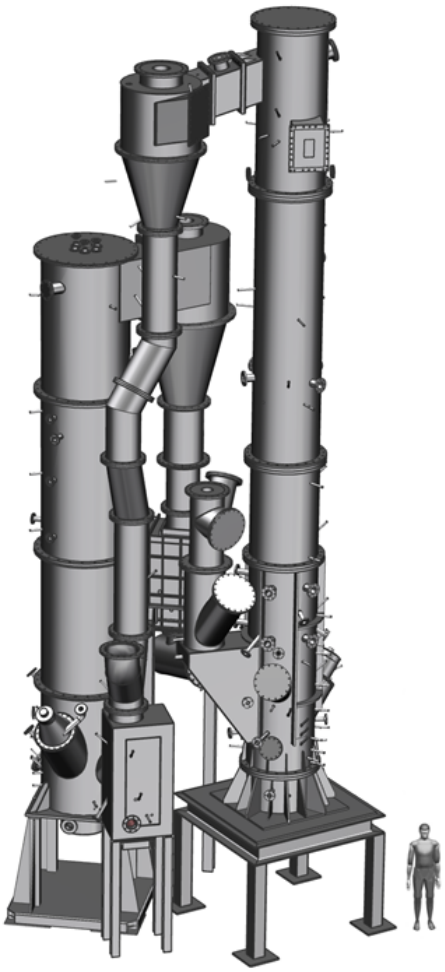

Figure 5. CLG reactor configuration including the main coupling elements.

Although many lab-scale reactor designs feature a FR operating in bubbling mode (e.g., [11,14,17,58]), the used CFB mode of the FR has the advantage of improved gas-solid mixing and thus featuring higher rates of carbon conversion [57], while the requirement ranges for the size and shape of the feedstock is wider [10] opening up possibilities for more feedstocks. Furthermore, the higher solids concentration in the freeboard may enhance tar cracking and methane reforming by supply of additional oxygen and catalytic sites in this region. However, increasing superficial velocities too much will lead to pneumatic transport in the FR (Figure 3) and unstable reactor hydrodynamics.

The disadvantage of having no internal solid recirculation for the FR is the transport of all discharged feedstock particles towards the AR. Furthermore, for the pilot plant, the minimization of heat losses is considered more important than the minimization of carbon slip towards the AR as relative heat losses for the pilot plant are in the range of 0.1 to 0.2. So minimization of coupling elements is used instead of carbon recovery via a carbon stripper. However, carbon slip is assumed to be a minor problem as the biomasses considered for the experiments contain low amounts of fixed carbon [9]. The feeding location is lowered into the dense region of the bed when compared to previous CLC experiments [49] where high carbon slip for hard coal was experienced, which should reduce the carbon slip as char gasification in the densest region is enhanced. Moreover,

carbon slip is more pronounced in small reactors and the sometimes utilized carbon strippers might not be required in bigger units [59]. Nonetheless, to maximize residence time of char particles inside the dense region, a variable amount of fluidization medium can be rerouted directly before the wind box of the FR to a second stage fluidization located at approx. one fifth of the reactor height. This increases bed density in the lower region and residence time of OC particles while keeping a high solids discharge in the CFB operation is possible by increasing the reactor inventory. The exact influence must be determined via experimental operation.

Investigations in the FR are the most crucial, as the formation of tars make the process and reactor design more critical to subsequent equipment than the re-oxidation in the AR. Therefore, it is advantageous for experimental operation to handle imbalances of solids discharge between the reactors inside the AR instead of the FR where it would negatively impact temperature and possibly lead to poorer syngas quality. The feedstock input directly in the dense zone of the bed should also reduce the amount of tars formed during initial devolatilization [37].

4.2. Flue Gas Handling

The flue gas composition from the AR is measured by an on-line gas analysis before the flue gas is cooled down in a heat exchanger to approx. 230 °C (Figure 4, red box). The flow rate is measured using a venturi before the fines passing the cyclone are separated by a filter giving a dust-free flue gas. The following induced draft fan is used to control the pressure in the reactor and vents the flue gas via a stack. Part of the flue gas can be recirculated via a controlled butterfly valve to adjust the inlet of the AR fluidization. The variation of flue gas recirculation allows to adjust the superficial gas velocity $u_{0,AR}$ and thereby the entrainment of particles from the AR while keeping the OC to fuel equivalence ratio ϕ constant. This is a small but significant adjustment in converting from a CLC plant to a CLG plant as it allows to control the overall process as described in [26].

4.3. Syngas Handling

Major modifications are needed for the FR off-gases (Figure 4, blue box) when converting a CLC unit into a CLG unit, as all parts need to be designed with the consideration of explosive atmospheres . Moreover, commonly used heat exchangers are either prone to clogging with tars on cold surfaces or the syngas cooling rate is to low, allowing for recombination of syngas species. The process simulation from Section 3.3 show high syngas streams that need to be safely handled and greatly exceed the capacity of the syngas removal deployed for HTW^{TM} gasification [45,46]. The only component reusable is the cooler, a patented tube-in-tube gas liquid heat exchanger from SCHMIDT'SCHE SCHACK consisting of four tubes cooling the gas to approx. 380 °C very fast and without recirculation zones [60] avoiding the recombination of syngas to longer hydro-carbons. The cooling water is pressurised to 28 bar to be able to raise temperature levels to 200 °C in order to avoid excessive condensation of tars inside the tubes of the raw gas cooler.

After the cooler the syngas is available for cleaning. Here part of the syngas can be routed to a syngas treatment unit for cleaning and separation of CO_2, so that it is subsequently available for synthesis. Moreover, test rigs for the fine cleaning of the syngas and the synthesis of higher hydro-carbons are added, creating the unique possibility to investigate the whole solid to liquid value chain.

The return line from the syngas treatment unit consisting of all streams not used for synthesis is merged back, and the gas is routed to a hot gas filter for the removal of solids, resulting in a dust free syngas stream to the hot syngas compressor used to control the pressure in the FR. From here the syngas is transported to a thermal oxidizer for safe venting. The option of a second stack where the FR off gas can be vented is included for start up, shut down and to allow for a restart of the thermal oxidizer in case of failures without the full shut down of the pilot plant. The additional valves before the hot gas filter

are installed for safety pressure relief in case the switching between the thermal oxidizer and the second stack fails.

The described syngas line differs substantially from the ones deployed in either industrial scale or lab-scale. While in industrial plants all produced syngas would be cleaned, only the amount of syngas needed for research in gas cleaning is processed in the pilot plant to reduce the cost of the deployed gas cleaning equipment. In lab-scale the small quantities of formed syngas allow for untreated release to a safe location in the environment, which is not possible for streams in the size of the pilot plant, entailing the need for the thermal oxidizer.

All properties of the syngas stream leaving the FR are of major importance for further process development. Thus, sample and measurement sites consisting of an isokinetic dust and tar sampling port, a psychrometric water content measurement, and an on-line gas analysis are integrated into the syngas line. The isokinetic sampling of dust and tars is done before the raw syngas is cooled while ports for the measurement of the water content and gas composition are located before and after the cooler and can be connected as required.

4.4. Solid Feeding

4.4.1. Feedstock

The pilot plant is equipped with various entry points for solid feedstocks (Figure 4, orange box) like a big bag station, a container station (not shown on Figure 4) and a silo capable of introducing pulverized and pelletized feedstocks which are transported pneumatically to a fuel container purged with CO_2. This container discontinuously feeds fuel to a second, weighted container from which the fuel is fed continuously, controlled via screws and a hopper directly in to the bed of the FR. Both containers are pressurised to the bed pressure of the FR at the location of the feed screw to avoid the back flow of syngas into the fuel feeding system. The screw feeder is cooled with thermal oil to ensure that gasification temperatures are only reached in the bed and no gasification occurs inside the screw.

4.4.2. Oxygen Carrier

Initial filling of loop seals with OC is done via a weighted dosing container, a hopper, a screw conveyor, and a series of tubs connected to the stand-pipes. OC materiel is fed into the return leg of LS 4.1 for reactor filling and make-up dosing to compensate losses caused by agglomeration and attrition.

4.5. Cooling and Preheating

The cooling system is designed to handle the full 1 MW of heat released during CLC and therefore has enough capacity for further increase of feedstock as discussed previously. However, for bigger units, where process heat would be used to generate steam and preheat the input streams, changes might be required when compared to CLC to optimize the heat integration. Nonetheless, this is no concern for the pilot plant, where steam generation and preheating is done via independently powered systems. Yet, it limits also the operation range of the pilot plant—seen on simulated case HT2—where higher outlet stream temperatures always lead to a severe process penalty. For the pilot plant, this penalty cannot be alleviated by heat recovery for the preheating of inlet streams. Here the option of higher preheating temperatures would require a substantial increase of heat exchanger surface, for which no space is available at the existing site. Furthermore, the existing electrical infrastructure is already at its limit, so increasing the electrical preheating power is not feasible.

Increasing the fuel input necessitates deeper investigation of the limitation of safe operation in terms of the cooling system, especially when considering that most of the 1000 kg OC material is in a highly reduced state during operation. Here the safety relevant quantity is not the total amount of feedstock input or the reduced OC, but the possible amount of oxygen input to the AR. The oxygen input will first fully oxidise the OC inside the AR, possibly with much higher power than the nominal feedstock input which will set a limit only after full oxidation inside the AR has been reached. Here mitigation measures are an over design of the cooling system and a limitation of oxygen input to safely handable amounts.

4.6. On Line Measurements

4.6.1. Gas Analysis

The main product of the gasification process, the synthesis gas from the FR, is extracted and analyzed continuously as sown in Figure 6 via a heated probe which includes a filter (1), that can be back flushed with CO_2 to prevent blockage.

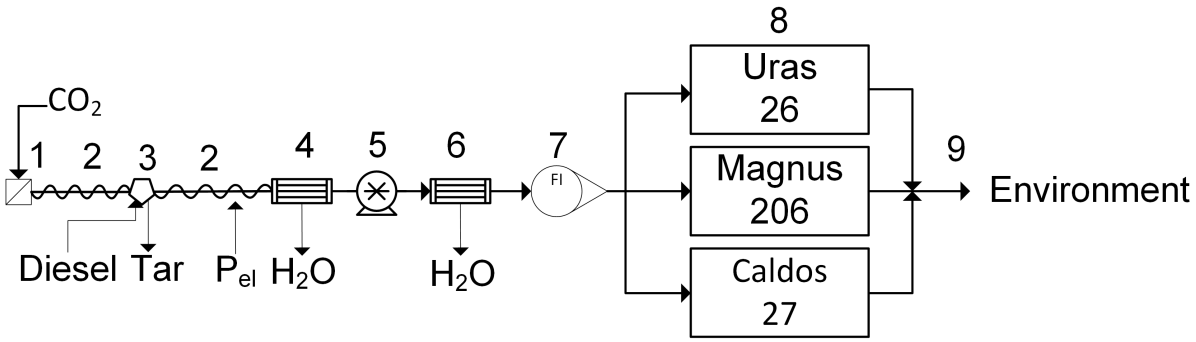

Figure 6. Schematic of the gas analysis equipment: (1) heated probe with filter, (2) heated tube, (3) tar removal (only for FR), (4) condenser for water removal, (5) pump, (6) condeser for water removal, (7) rotameter, (8) measurement equipment, (9) safe location in the environment.

The gas then passes in a heated tube (2)—to prevent the condensation of remaining tars—to a tar removal unit with diesel as solvent (3) and a first condenser unit (4) where the majority of the water and higher hydro-carbons are removed. The measurement gas pump (5) transports the gas through a second condenser unit to remove the rest of the water (6) which is followed by a rotameter (7) measuring the sampling gas flow. The sampling gas is distributed to the commercially available gas analysing equipment from ABB (8) given in Table 5 before being released to a safe location in the environment (9).

O_2 is measured via its paramagnetic quality in an Magnos 206 analyzer while H_2 is determined via thermal conductivity in a Caldos 27 unit. The components CO_2, CO, CH_4, SO_2 and NO are measured by an spectroscopic non-dispersive infra red (NDIR) sensor in an Uras 26 analyzer.

For the AR both gas analysis lines differ in the heated probe which does not include a tar removal unit. The measurement ranges of the equipment is different, as can be seen in Table 5 and H_2 and CH_4 is not measured. At the inlet of the AR, the composition is of interest to control the oxygen feed to the process and the amount of recirculated flue gas.

The water content is measured in both reactor outlets via a psychrometric Hygrophil H4320 unit from Bartec with the sampling gas extraction as shown in Figure 7. The gas is extracted via a heated probe (1) and transported in an electrically heated tube (2) to the analyzer (3) which includes a CO_2-driven ejector pump to facilitate the gas transport. The gas is released to the environment afterwards (4).

Table 5. Listing of gas analysis equipment for all reactors.

Reactor	Equipment	Measurement Principle	Component	Range	Error	Unit
FR	Magnos 206	paramagnetic	O_2	0 to 25	0.9	vol. − %
	Caldos 27	thermal conductivity	H_2	0 to 40	1.8	vol. − %
	Uras 26	NDIR	CO_2	0 to 100	3.0	vol. − %
	Uras 26	NDIR	CO	0 to 40	1.2	vol. − %
	Uras 26	NDIR	CH_4	0 to 20	0.6	vol. − %
	Uras 26	NDIR	SO_2	0 to 5	0.15	vol. − %
	Uras 26	NDIR	NO	0 to 1000	30	ppm
	Hygrophil H4320	psychrometric	H_2O	2 to 100	0.3	vol. − %
AR outlet	Magnos 206	paramagnetic	O_2	0 to 25	0.9	vol. − %
	Uras 26	NDIR	CO_2	0 to 30	0.9	vol. − %
	Uras 26	NDIR	CO	0 to 5	0.15	vol. − %
	Uras 26	NDIR	SO_2	0 to 4000	120	ppm
	Uras 26	NDIR	NO	0 to 1000	30	ppm
	Hygrophil H4320	psychrometric	H_2O	2 to 100	0.3	vol. − %
AR inlet	Magnos 206	paramagnetic	O_2	0 to 25	0.9	vol. − %
	Uras 26	NDIR	CO_2	0 to 100	3.0	vol. − %
	Uras 26	NDIR	CO	0 to 5	0.15	vol. − %
	Uras 26	NDIR	SO_2	0 to 5	0.15	vol. − %
	Uras 26	NDIR	NO	0 to 1000	30	ppm

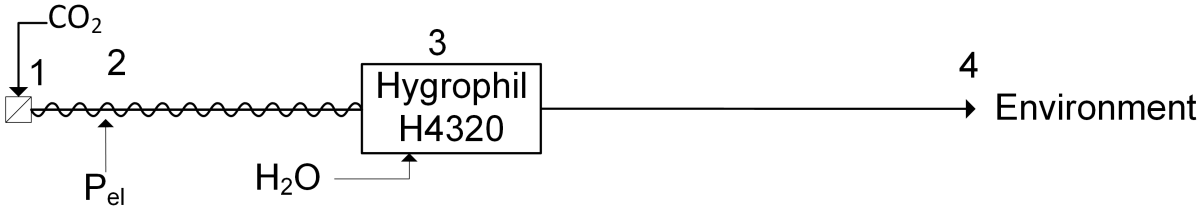

Figure 7. Schematic of the water content analysis equipment: (1) heated probe with filter, (2) heated tube, (3) psychrometric analyzer, (4) safe location in the environment.

Both water content measurements and the three gas analysis are integrated in the process control system of the pilot plant with all measurements available in real time and as trend lines.

4.6.2. Temperature and Pressure

The pilot is equipped with temperature and pressure in all inlet and outlet streams of the reactors including the LS fluidization. Multiple additional measurement sites for pressure and temperature are installed along the reactor height to acquire more insight in the reactor state during operation. The pressure sensors for the AR are differential pressure transducers with the other side open to atmosphere while at the FR all pressure measurements are purged with CO_2 and are mostly differential pressure transducers measuring between different reactor heights. This allows us to control the bed hight and density and to control the influence of the second stage fluidization.

4.6.3. Flow Measurements

The flow rates of all streams entering the reactors and coupling elements are measured either with an orifice plate, a rotameter or are controlled via a mass flow controller. The main streams leaving the reactors are measured via two venturi with side streams for off-line analysis, process control or the syngas treatment unit measured inside the respective analysis or control equipment. The mass flow of solids entering the system is measured via load cells and the corresponding trend line gradients.

4.7. Off-Line Sampling

4.7.1. Solid Sampling

The bottom product removal of the AR transfers the material to an open barrel and is immediately accessible for inspection and sampling, while for the FR it is transferred to a sealed and CO_2-purged container which can be replaced periodically during operation to allow for the collection of samples. The same is implemented for filter dust sampling. The AR filter is equipped with a hopper and an open barrel, while the FR filter has an additional CO_2 purge and the container is sealed.

Both loop seals allow for the collection of solid samples for off-line analysis. The OC samples enable the determination of the exact phase composition of the circulating OC and to balance the reactors individually. Moreover, knowledge of the oxidation level before and after the reactors allows for an additional method for the quantification of solid circulation.

4.7.2. Gas and Tar Sampling

More gas species like COS and higher hydrocarbons can be measured using Fourier transform infrared (FTIR) spectroscopy which can be connected at different locations. These measurements are not considered important during pilot plant operation but are important for the evaluation of the process. At the FTIR a port for gas sample bags and gas mice exists to enable off-line gas analysis.

Additionally, isokinetic sampling is possible in the synthesis gas line allowing for dust and tar sample collection according to tar protocol/CEN TS 15439. Velocity is measured by an S-Pitot tube 550 mm downstream of the sampling lance, both located in the center line of a refractory lined tube. The dust loaded syngas sample stream is transfered via a heated lance towards a heated filter and through six impinger bottles where five are filled with isopropanol as solvent and the last is empty. The impinger bottles are tempered to 40 °C (impinger 1, 2 and 4) and −20 °C (impinger 2, 5 and 6). The sample volume is measured inside a comercially available ST5 isokinetic sampler from Dado lab, which also adjusts the sample volume flow based on the pitot measurement.

5. Plant Operation

The simulations from Section 3.3 show that autothermal CLG experiments are needed to obtain further insights into the process, which are of high relevance for industrial deployment. The modified pilot plant (Section 4) renders these experiments feasible allowing for the generation of the following, required information:

5.1. Literature, describing the demonstration of autothermal operation of the CLG process, is not yet available. While autothermal CLC has been successfully demonstrated [49,51] the higher prevalence of endothermic reactions impose the need for higher heat transfer to the FR and different control strategies [26].

5.2. Continuous CLG of residual biomass has been successfully demonstrated in lab-scale [11,15,16]. Nonetheless, upscaling to higher thermal loads is necessary to obtain data for reliable simulations and design of industrial scale units.

5.3. Due to their interdependence, the key performance indicators achievable in autothermal operation are unknown. This affects the cold gas efficiency η_{CG}, the carbon conversion η_{CC}, the syngas yield x_{SG} and the syngas quality (tars, CH_4, etc.). For example, in electrically heated systems the cold gas efficiency η_{CG} can be theoretically driven to 100% by supplying enough heat through the furnace. However, the exact amount of external heat supplied is seldom reported. The carbon slip depends amongst other on reactor size [59] and data for bigger scale units is not existent.

5.4. Tar production can presently not be accurately predicted as no model was developed for CLG yet. Especially bed height and feeding location are also dependent on reactor size and their influence cannot be quantified [37]. The pilot plant experiments will give important insight on this matter in industrial like conditions, allowing for inferences for future upscaling endeavours.

5.5. OC life time is difficult to asses with currently available data, as the time of circulation and thus of re-oxidation cycles increases with increasing reactor size while the mechanical erosion is dependent on the transport velocity only. The exact contribution of the two effects is unknown and thus it is likely that the size of the reactor will have an influence on the OC life time.

5.6. Assessment of economic feasibility of the CLG process requires data from bigger scale units to make accurate predictions for e.g., sizing of components and process performance.

For the demonstration of autothermal CLG (item 5.1.) a suitable control concept for the oxygen carrier to fuel equivalence ratio ϕ based on a sub-stoichiometric AR operation (reduced OC oxidation, see Equations (2) and (3)) according to Dieringer et al. [26] is implemented. The corresponding operating strategy considering pilot plant limitations is described in the following.

Chemical Looping Gasification Operation

The start-up sequence of the pilot plant is preheating with electrically heated air, preheating with propane burner, OC filling plus propane burner, CFB combustion, CLC as described in [47]. Afterwards the switch to CLG is achieved by a reduction of air input to the AR while increasing flue gas recirculation, thus reducing ϕ to values smaller than unity. After stable CLG operation is attained, optimization of individual key performance indicators is targeted during experiments. The devised experimental operation of the pilot plant (described hereafter) allows to directly obtain data for items 5.2. and 5.3. while information for items 5.4. and 5.5. can be inferred from additional off-line analysis. Item 5.6. builds on this data but needs additional information, e.g., component and material pricing, which cannot be generated in the pilot plant. The main operation variables through which the process can be controlled are:

- Thermal load: Increasing the thermal load above 1 MW_{th} decreases the relative heat loss as it depends on reactor temperature and not on thermal load. Therefore, a higher fraction of the feedstock input, $\dot{m}_{FS}$, can be converted into syngas increasing process efficiency. The feedstock input rate $\dot{m}_{FS}$ is directly proportional to the thermal load, but an adjustment requires corresponding changes in fluidization imposed by reactor hydrodynamics and heat balance influencing the steam to biomass ratio. Nonetheless, the simulations in Section 3.3 show also an increase of CH_4 production with increasing thermal load, indicating a tendency to form hydrocarbons including tars.
  The limit for the thermal input is set by the maximum possible feedstock input and the syngas handling and cooling, as higher loads result in a higher amount of product gas which has to be handled safely. During operation a high thermal load is targeted at all operation points to obtain high η_{CG}.
- The OC to fuel equivalence ratio ϕ determines the net heat release from the process. A higher value of ϕ (while keeping everything else constant) results in a higher temperature inside AR and FR. However, the cold gas efficiency η_{CG} will decrease with higher ϕ as does the production of CH_4 and tars. The control of ϕ is straightforward through the control of the oxygen availability inside the AR.
  For experimental investigation the variation of temperatures is important. However, higher temperatures increase the load on the cooling system. Here the limits have to be considered during operation, and a reduction in thermal load (leading to smaller process streams and further decreasing η_{CG}) may be required in order to be able to reach higher gasification temperatures. Moreover, the refractory lining of the AR and/or the ash melting behaviour of the feedstock inside the FR limit the maximum admissible reactor temperatures.
  Actual control of ϕ is achieved via the variable amounts of air and recirculated AR flue gas fed to the AR to obtain a sub-stoichiometric environment inside the AR as it is the most suitable method for large scale operation described in detail by Dieringer et al. [26].

- The global solids circulation $\dot{m}_{OC}$ can be controlled via adjustment of J-valve and FR fluidization and transports sensible heat required in the FR. Depending on the operating state of the AR internal solids recirculation, fluidization of the AR needs adjustment as well to obtain hydrodynamic equilibrium between the reactors. Yet, $\dot{m}_{OC}$ is not directly accessible during pilot plant operation but can be inferred qualitatively from the temperature difference between the reactors. Higher solids circulation reduces the temperature difference ΔT between AR and FR. An accurate determination of $\dot{m}_{OC}$ is possible only indirectly via the oxygen content in the solid samples taken from the loop seals.
  Increasing global solids circulation reduces not only ΔT but also η_{CG} as more fluidization medium and corresponding heating is required. Furthermore, OC residence time inside the reactors is reduced when the solids circulation increases and as higher superficial gas velocities are employed, carbon slip towards the AR might increase. The variable to be controlled is the gasification temperature inside the FR while the limit of the AR temperature might require adjustment via ϕ.

The OC to fuel equivalence ratio ϕ and the global solids circulation $\dot{m}_{OC}$ are used to investigate the inevitable trade-off between cold gas efficiency and syngas quality in the form of produced CH_4, higher hydrocarbons, and tar. In contrast, the maximization of the thermal load is used to boost the process performance η_{CG} for all operation points by allowing for a smaller value of ϕ while at the same time guaranteeing autothermal operation.

While the variables above are used to adjust and stabilize the process and to investigate general trends, two more adjustable parameters exist which can be used to influence the syngas quality:

- Bed pressure drop Δp: The simulations in Section 3.3 are done with a fixed pressure drop Δp for both reactors. However, during operation of the pilot plant, Δp can be varied and is dependent on the exact distribution of bed material between the reactors (controlled by the governing hydrodynamic boundary conditions) as well as the total amount of bed material inside the reactor system. Increasing the pressure drop inside the FR will increase OC particle residence time inside the reactor (and the amount of OC per feedstock input). This will also increase the entrainment from the FR and thereby the solid circulation. However, increasing Δp allows for the reduction of fluidization medium, while keeping the entrainment constant, thus improving process efficiency. Reduction of tar and CH_4 content in syngas is facilitated by the increased availability of catalytic sites for conversion.
  The OC make up stream is used to control the overall amount of OC inside the reactor system, while its distribution is influenced by small adjustments to fluidization medium. The required changes in fluidization are small compared to the changes needed for the operation variables discussed above. The range of Δp is limited by the reactor hydrodynamics and the characteristics of corresponding pripheral equipment (e.g., maximum load of AR primary air fan).
- Second stage fluidization can be varied to enhance the residence time of the feedstock inside the dense zone of the FR as describes in Section 4.1. Rerouting part of the fluidization medium to the second stage fluidization will reduce entrainment and solid circulation, if the total amount of steam is kept constant and can be counteracted by additional bed material. Qualitative effects on synthesis gas are the same as for the bed pressure drop Δp, however, the quantitative influence may vary.

The feedstock types given in Table 2 are an additional parameter for experimental variation. However, the feedstock is not usable as process control variable and is therefore not included in the list above. Furthermore, the other variables must be used to adjust for feedstock variation to keep the process stable.

6. Conclusions

In this article, the design pathway of a 1 MW_{th} chemical looping gasification (CLG) pilot plant, allowing for autothermal, semi-industrial process investigation, has been described in detail. Starting from a process model, considering fundamental CLG characteristics, a suitable operational mode and associated necessary adaptions for an existing 1 MW_{th} chemical looping combustion (CLC) pilot plant have been established. Subsequently, it has been illustrated which inherent interconnections and trade-offs associated to CLG can be further analyzed in such an experimental setup and which strategies towards an optimized process setup, replicable in industry scale, can be pursued with it. These are:

- Calculation of heat and mass balances for autothermal CLG show a significantly reduced range of freely selectable operation parameters (operation temperatures, steam to biomass feed ratio, and oxygen carrier to fuel equivalence ratio), when compared to externally heated lab-scale units, due to the requirements of autothermal operation.
- Process control under autothermal condition can be achieved via three parameters: thermal load, oxygen carrier to fuel equivalence ratio, and global solid circulation. However, due to restrictions imposed by reactor hydrodynamics and autothermal operation, changes in one parameter must be balanced by changes in at least one of the other two. Moreover, the global solids circulation is adjusted indirectly via fluidization velocities and can only be inferred qualitatively from the reactor temperature difference during operation.
- Attempting to attain high cold gas efficiency and good syngas quality through higher gasification temperature inevitably results in high relative heat losses, as heat integration is not reasonably achievable in the 1 MW_{th} scale and the existing unit. This leads to an unavoidable trade-off between cold gas efficiency and syngas quality, e.g., CH_4 and tar content which has to be accepted during experiments.
- Data which are not reliably obtainable from simulation, like tar formation or oxygen carrier (OC) life time, yet are fundamental for scale-up and economic considerations becomes available by conducting experiments in an industry relevant scale in the designed pilot plant.

In summary, future endeavours aiming towards industrial application of CLG are facilitated, through the described design of a 1 MW_{th} CLG pilot plant. Here, the experimental facility lays the foundation to generate a unique robust dataset containing essential information required for up-scaling of CLG to industry size, thus propelling the technology towards market maturity.

Author Contributions: Conceptualization, F.M., J.S. and P.D.; simulation, P.D. and F.M.; writing—original draft preparation, F.M.; writing—review and editing, P.D., J.S. and F.M.; visualization, F.M. and P.D.; supervision, B.E. All authors have read and agreed to the published version of the manuscript.

Funding: This work has received funding of the European Union's Horizon 2020—Research and Innovation Framework Programme under grant agreement No. 817841 (Chemical Looping gasification foR sustainAble production of biofuels—CLARA).

Acknowledgments: The authors gratefully acknowledge the support given by Harald Tremmel and Karl Voigtländer from AICHERNIG Engineering GmbH during HAZOP analysis.

Conflicts of Interest: The authors declare no conflict of interest.

Abbreviations

The following abbreviations are used in this manuscript:

AR	air reactor
ASU	air separation unit
CFB	circulating fluidized bed
CLC	chemical looping combustion
CLG	chemical looping gasification
CLOU	chemical looping with oxygen uncoupling
DFBG	dual fluidized bed gasification
FR	fuel reactor
FTIR	Fourier transform infrared
HTW^{TM}	High Temperature Winkler
LS	loop seal
NDIR	non-dispersive infra red
OC	oxygen carrier

Symbols

LHV	MJ kg^{-1}, MJ mol^{-1}	lower heating value
R_{OC}		oxygen transport capacity
T	K, °C	temperature
X		mole fraction
ΔH	J mol^{-1}	reaction enthalpy
Δp	Pa, bar	differential pressure
ϕ		oxygen carrier to fuel equivalence ratio
$\dot{Q}$	W	heat flow
$\dot{m}$	kg s^{-1}	mass flow
$\dot{n}$	mol s^{-1}	molar flow
η_{CG}		cold gas efficiency
c_p	J kg^{-1} K^{-1}	specific heat
$d_{p,50}$	m	mean particle diameter
d	m	diameter
h	m	height
m	kg	mass
p	Pa, bar	pressure
u	m s^{-1}	velocity
x_{SG}		syngas content

Subscripts

AR	Air Reactor
FR	Fuel Reactor
FS	Feed Stock
OC	Oxygen Carrier
O	Oxygen
internal	internal recirculation
in	stream entering reactor
loss	loss
out	stream leaving reactor
ox	oxidized
reci	recirculation
red	reduced
stoich	stoichiometric

References

1. Directive (EU) 2018/2001 of the European Parliament and of the Council of 11 December 2018 on the Promotion of the Use of Energy from Renewable Sources. p. 128. Available online: https://eurovent.eu/?q=articles/review-directive-eu-20182001-promotion-use-energy-renewable-sources-gen-115400 (accessed on 19 December 2020).

2. International Energy Agency. Data & Statistics. 2020. Available online: https://www.iea.org/data-and-statistics?country=EU28&fuel=Energy20transition20indicators&indicator=Biotrans (accessed on 19 December 2020).
3. Kaltschmitt, M. (Ed.) *Energy from Organic Materials (Biomass): A Volume in the Encyclopedia of Sustainability Science and Technology*, 2nd ed.; Springer: New York, NY, USA, 2019. doi:10.1007/978-1-4939-7813-7.
4. Carrasco, J.E.; Monti, A.; Tayeb, J.; Kiel, J.; Girio, F.; Matas, B.; Santos Jorge, R. Strategic Research and Innovation Agenda 2020. EERA Technical Report. 2020. Available online: http://www.eera-bioenergy.eu/wp-content/uploads/pdf/EERABioenergySRIA2020.pdf=AOvVaw012VUhnaqiUbL-yP76cz6s (accessed on 19 December 2020).
5. Molino, A.; Larocca, V.; Chianese, S.; Musmarra, D. Biofuels Production by Biomass Gasification: A Review. *Energies* **2018**, *11*, 811, doi:10.3390/en11040811.
6. Gómez-Barea, A.; Leckner, B. Estimation of Gas Composition and Char Conversion in a Fluidized Bed Biomass Gasifier. *Fuel* **2013**, *107*, 419–431, doi:10.1016/j.fuel.2012.09.084.
7. Thomsen, T.P.; Sárossy, Z.; Gøbel, B.; Stoholm, P.; Ahrenfeldt, J.; Frandsen, F.J.; Henriksen, U.B. Low Temperature Circulating Fluidized Bed Gasification and Co-Gasification of Municipal Sewage Sludge. Part 1: Process Performance and Gas Product Characterization. *Waste Manag.* **2017**, *66*, 123–133, doi:10.1016/j.wasman.2017.04.028.
8. Arena, U.; Zaccariello, L.; Mastellone, M.L. Fluidized Bed Gasification of Waste-Derived Fuels. *Waste Manag.* **2010**, *30*, 1212–1219, doi:10.1016/j.wasman.2010.01.038.
9. De, S.; Agarwal, A.K.; Moholkar, V.S.; Thallada, B. (Eds.) *Coal and Biomass Gasification: Recent Advances and Future Challenges*; Energy, Environment, and Sustainability; Springer: Singapore, 2018, doi:10.1007/978-981-10-7335-9.
10. Higman, C.; van der Burgt, M. *Gasification*, 2nd ed.; Gulf Professional Pub.: Boston, MA, USA; Elsevier: Amsterdam, The Netherlands, 2008.
11. Condori, O.; García-Labiano, F.; de Diego, L.F.; Izquierdo, M.T.; Abad, A.; Adánez, J. Biomass Chemical Looping Gasification for Syngas Production Using Ilmenite as Oxygen Carrier in a 1.5 kWth Unit. *Chem. Eng. J.* **2021**, *405*, 126679, doi:10.1016/j.cej.2020.126679.
12. Huseyin, S.; Wei, G.Q.; Li, H.B.; He, F.; Huang, Z. Chemical-Looping Gasification of Biomass in a 10 kWth Interconnected Fluidized Bed Reactor Using Fe_2O_3/Al_2O_3 Oxygen Carrier. *J. Fuel Chem. Technol.* **2014**, *42*, 922–931, doi:10.1016/S1872-5813(14)60039-6.
13. Guo, Q.; Cheng, Y.; Liu, Y.; Jia, W.; Ryu, H.J. Coal Chemical Looping Gasification for Syngas Generation Using an Iron-Based Oxygen Carrier. *Ind. Eng. Chem. Res.* **2014**, *53*, 78–86, doi:10.1021/ie401568x.
14. Wei, G.; He, F.; Huang, Z.; Zheng, A.; Zhao, K.; Li, H. Continuous Operation of a 10 kW_{th} Chemical Looping Integrated Fluidized Bed Reactor for Gasifying Biomass Using an Iron-Based Oxygen Carrier. *Energy Fuels* **2015**, *29*, 233–241, doi:10.1021/ef5021457.
15. Samprón, I.; de Diego, L.F.; García-Labiano, F.; Izquierdo, M.T.; Abad, A.; Adánez, J. Biomass Chemical Looping Gasification of Pine Wood Using a Synthetic Fe_2O_3/Al_2O_3 Oxygen Carrier in a Continuous Unit. *Bioresour. Technol.* **2020**, *316*, 123908, doi:10.1016/j.biortech.2020.123908.
16. Ge, H.; Guo, W.; Shen, L.; Song, T.; Xiao, J. Experimental Investigation on Biomass Gasification Using Chemical Looping in a Batch Reactor and a Continuous Dual Reactor. *Chem. Eng. J.* **2016**, *286*, 689–700, doi:10.1016/j.cej.2015.11.008.
17. Ge, H.; Guo, W.; Shen, L.; Song, T.; Xiao, J. Biomass Gasification Using Chemical Looping in a 25 kW Th Reactor with Natural Hematite as Oxygen Carrier. *Chem. Eng. J.* **2016**, *286*, 174–183, doi:10.1016/j.cej.2015.10.092.
18. Brown, T.A.; Dennis, J.S.; Scott, S.A.; Davidson, J.F.; Hayhurst, A.N. Gasification and Chemical-Looping Combustion of a Lignite Char in a Fluidized Bed of Iron Oxide. *Energy Fuels* **2010**, *24*, 3034–3048, doi:10.1021/ef100068m.
19. Leion, H.; Mattisson, T.; Lyngfelt, A. The Use of Petroleum Coke as Fuel in Chemical-Looping Combustion. *Fuel* **2007**, *86*, 1947–1958, doi:10.1016/j.fuel.2006.11.037.
20. Chen, L. The Direct Solid-Solid Reaction between Coal Char and Iron-Based Oxygen Carrier and Its Contribution to Solid-Fueled Chemical Looping Combustion. *Appl. Energy* **2016**, *184*, 9–18. doi:10.1016/j.apenergy.2016.09.085.
21. Leion, H.; Mattisson, T.; Lyngfelt, A. Solid Fuels in Chemical-Looping Combustion. *Int. J. Greenh. Gas Control* **2008**, *2*, 180–193, doi:10.1016/S1750-5836(07)00117-X.
22. Song, Q.; Xiao, R.; Deng, Z.; Zhang, H.; Shen, L.; Xiao, J.; Zhang, M. Chemical-Looping Combustion of Methane with $CaSO_4$ Oxygen Carrier in a Fixed Bed Reactor. *Energy Convers. Manag.* **2008**, *49*, 3178–3187, doi:10.1016/j.enconman.2008.05.020.
23. Pissot, S.; Vilches, T.B.; Maric, J.; Seemann, M. Chemical Looping Gasification in a 2–4 MWth Dual Fluidized Bed Gasifier. In Proceedings of the 23rd International Conference on Fluidized Bed Conversion, Seoul, Korea, 13–17 May 2018; p. 10.
24. Larsson, A.; Seemann, M.; Neves, D.; Thunman, H. Evaluation of Performance of Industrial-Scale Dual Fluidized Bed Gasifiers Using the Chalmers 2–4-MW_{th} Gasifier. *Energy Fuels* **2013**, *27*, 6665–6680, doi:10.1021/ef400981j.
25. Larsson, A.; Israelsson, M.; Lind, F.; Seemann, M.; Thunman, H. Using Ilmenite to Reduce the Tar Yield in a Dual Fluidized Bed Gasification System. *Energy Fuels* **2014**, *28*, 2632–2644, doi:10.1021/ef500132p.
26. Dieringer, P.; Marx, F.; Alobaid, F.; Ströhle, J.; Epple, B. Process Control Strategies in Chemical Looping Gasification—A Novel Process for the Production of Biofuels Allowing for Net Negative CO_2 Emissions. *Appl. Sci.* **2020**, *10*, 26, doi:10.3390/app10124271.
27. Yin, S.; Shen, L.; Dosta, M.; Hartge, E.U.; Heinrich, S.; Lu, P.; Werther, J.; Song, T. Chemical Looping Gasification of a Biomass Pellet with a Manganese Ore as an Oxygen Carrier in the Fluidized Bed. *Energy Fuels* **2018**, *32*, 11. doi:10.1021/acs.energyfuels.8b02849.
28. Adanez, J.; Abad, A.; Garcia-Labiano, F.; Gayan, P.; de Diego, L.F. Progress in Chemical-Looping Combustion and Reforming Technologies. *Prog. Energy Combust. Sci.* **2012**, *38*, 215–282, doi:10.1016/j.pecs.2011.09.001.

29. Linderholm, C.; Knutsson, P.; Schmitz, M.; Markström, P.; Lyngfelt, A. Material Balances of Carbon, Sulfur, Nitrogen and Ilmenite in a 100 kW CLC Reactor System. *Int. J. Greenh. Gas Control* **2014**, *27*, 188–202, doi:10.1016/j.ijggc.2014.05.001.
30. Alabdrabalameer, H.A.; Taylor, M.J.; Kauppinen, J.; Soini, T.; Pikkarainen, T.; Skoulou, V. Big Problem, Little Answer: Overcoming Bed Agglomeration and Reactor Slagging during the Gasification of Barley Straw under Continuous Operation. *Sustain. Energy Fuels* **2020**, *4*, 3764–3772, doi:10.1039/D0SE00155D.
31. Di Giuliano, A.; Funcia, I.; Pérez-Vega, R.; Gil, J.; Gallucci, K. Novel Application of Pretreatment and Diagnostic Method Using Dynamic Pressure Fluctuations to Resolve and Detect Issues Related to Biogenic Residue Ash in Chemical Looping Gasification. *Processes* **2020**, *8*, 1137, doi:10.3390/pr8091137.
32. Fernández, M.J. Sintering reduction of herbaceous biomass when blended with woody biomass: Predictive and combustion tests. *Fuel* **2019**, *239*, 1115–1124, doi:10.1016/j.fuel.2018.11.115.
33. Luo, S.; Zeng, L.; Fan, L.S. Chemical Looping Technology: Oxygen Carrier Characteristics. *Annu. Rev. Chem. Biomol. Eng.* **2015**, *6*, 53–75, doi:10.1146/annurev-chembioeng-060713-040334.
34. Fan, L.S.; Zeng, L.; Luo, S. Chemical-Looping Technology Platform. *AIChE J.* **2015**, *61*, 2–22, doi:10.1002/aic.14695.
35. Zhao, X.; Zhou, H.; Sikarwar, V.S.; Zhao, M.; Park, A.H.A.; Fennell, P.S.; Shen, L.; Fan, L.S. Biomass-Based Chemical Looping Technologies: The Good, the Bad and the Future. *Energy Environ. Sci.* **2017**, *10*, 1885–1910, doi:10.1039/C6EE03718F.
36. Larsson, A.; Kuba, M.; Berdugo Vilches, T.; Seemann, M.; Hofbauer, H.; Thunman, H. Steam Gasification of Biomass—Typical Gas Quality and Operational Strategies Derived from Industrial-Scale Plants. *Fuel Process. Technol.* **2021**, *212*, 106609, doi:10.1016/j.fuproc.2020.106609.
37. Gómez-Barea, A.; Ollero, P.; Leckner, B. Optimization of Char and Tar Conversion in Fluidized Bed Biomass Gasifiers. *Fuel* **2013**, *103*, 42–52, doi:10.1016/j.fuel.2011.04.042.
38. Devi, L.; Ptasinski, K.J.; Janssen, F.J. Pretreated Olivine as Tar Removal Catalyst for Biomass Gasifiers: Investigation Using Naphthalene as Model Biomass Tar. *Fuel Process. Technol.* **2005**, *86*, 707–730, doi:10.1016/j.fuproc.2004.07.001.
39. Amin, A.M.; Croiset, E.; Epling, W. Review of Methane Catalytic Cracking for Hydrogen Production. *Int. J. Hydrogen Energy* **2011**, *36*, 2904–2935, doi:10.1016/j.ijhydene.2010.11.035.
40. Milne, T.A.; Evans, R.J.; Abatzaglou, N. *Biomass Gasifier "Tars": Their Nature, Formation, and Conversion*; Technical Report NREL/TP-570-25357; United States Department of Energy: Washington, DC, USA, 1998. doi:10.2172/3726.
41. Benedikt, F.; Kuba, M.; Schmid, J.C.; Müller, S.; Hofbauer, H. Assessment of Correlations between Tar and Product Gas Composition in Dual Fluidized Bed Steam Gasification for Online Tar Prediction. *Appl. Energy* **2019**, *238*, 1138–1149, doi:10.1016/j.apenergy.2019.01.181.
42. Palma, C.F. Model for Biomass Gasification Including Tar Formation and Evolution. *Energy Fuels* **2013**, *27*, 5. doi:10.1021/ef4004297.
43. Wojnicka, B.; Ściążko, M.; Schmid, J.C. Modelling of Biomass Gasification with Steam. *Biomass Conv. Bioref.* **2019**, doi:10.1007/s13399-019-00575-2.
44. Stark, A.K.; Bates, R.B.; Zhao, Z.; Ghoniem, A.F. Prediction and Validation of Major Gas and Tar Species from a Reactor Network Model of Air-Blown Fluidized Bed Biomass Gasification. *Energy Fuels* **2015**, *29*, 2437–2452, doi:10.1021/ef5027955.
45. Herdel, P.; Krause, D.; Peters, J.; Kolmorgen, B.; Ströhle, J.; Epple, B. Experimental Investigations in a Demonstration Plant for Fluidized Bed Gasification of Multiple Feedstock's in 0.5 MW Th Scale. *Fuel* **2017**, *205*, 286–296, doi:10.1016/j.fuel.2017.05.058.
46. Krause, D.; Herdel, P.; Ströhle, J.; Epple, B. HTW™-Gasification of High Volatile Bituminous Coal in a 500 kWth Pilot Plant. *Fuel* **2019**, *250*, 306–314, doi:10.1016/j.fuel.2019.04.014.
47. Ströhle, J.; Orth, M.; Epple, B. Design and Operation of a 1 MWth Chemical Looping Plant. *Appl. Energy* **2014**, *113*, 1490–1495, doi:10.1016/j.apenergy.2013.09.008.
48. Ströhle, J.; Orth, M.; Epple, B. Chemical Looping Combustion of Hard Coal in a 1 MWth Pilot Plant Using Ilmenite as Oxygen Carrier. *Appl. Energy* **2015**, *157*, 288–294, doi:10.1016/j.apenergy.2015.06.035.
49. Ohlemüller, P.; Busch, J.P.; Reitz, M.; Ströhle, J.; Epple, B. Chemical-Looping Combustion of Hard Coal: Autothermal Operation of a 1 MWth Pilot Plant. *J. Energy Resour. Technol.* **2016**, *138*, 042203, doi:10.1115/1.4032357.
50. Ohlemüller, P.; Ströhle, J.; Epple, B. Chemical Looping Combustion of Hard Coal and Torrefied Biomass in a 1 MW Th Pilot Plant. *Int. J. Greenh. Gas Control* **2017**, *65*, 149–159, doi:10.1016/j.ijggc.2017.08.013.
51. Ohlemüller, P.; Alobaid, F.; Abad, A.; Adanez, J.; Ströhle, J.; Epple, B. Development and Validation of a 1D Process Model with Autothermal Operation of a 1 MW Th Chemical Looping Pilot Plant. *Int. J. Greenh. Gas Control* **2018**, *73*, 29–41, doi:10.1016/j.ijggc.2018.03.013.
52. Min, Z.; Asadullah, M.; Yimsiri, P.; Zhang, S.; Wu, H.; Li, C.Z. Catalytic Reforming of Tar during Gasification. Part I. Steam Reforming of Biomass Tar Using Ilmenite as a Catalyst. *Fuel* **2011**, *90*, 1847–1854, doi:10.1016/j.fuel.2010.12.039.
53. Di Giuliano, A.; Lucantonio, S.; Gallucci, K. Devolatilization of Residual Biomasses for Chemical Looping Gasification in Fluidized Beds Made up of Oxygen-Carriers. *Energies* **2021**, *14*, 311, doi:10.3390/en14020311.
54. Kunii, D.; Levenspiel, O. *Fluidization Engineering*, 2nd ed.; Butterworth-Heinemann Series in Chemical Engineering; Butterworth-Heinemann: Boston, MA, USA, 1991.
55. Ohlemüller, P.; Alobaid, F.; Gunnarsson, A.; Ströhle, J.; Epple, B. Development of a Process Model for Coal Chemical Looping Combustion and Validation against 100 kWth Tests. *Appl. Energy* **2015**, *157*, 433–448, doi:10.1016/j.apenergy.2015.05.088.
56. Grace, J.R.; Avidan, A.A.; Knowlton, T.M. (Eds.) *Circulating Fluidized Beds*, 1st ed.; Blackie Academic & Professional: London, UK; New York, NY, USA, 1997.

57. Schmid, J.C.; Pfeifer, C.; Kitzler, H.; Pröll, T.; Hofbauer, H. A New Dual Fluidized Bed Gasifier Design for Improved in Situ Conversion of Hydrocarbons. In Proceedings of the International Conference on Polygeneration Strategies (ICPS), Vienna, Austria, 30 August–1 September 2011; p. 10.
58. Kronberger, B.; Johansson, E.; Löffler, G.; Mattisson, T.; Lyngfelt, A.; Hofbauer, H. A Two-Compartment Fluidized Bed Reactor for CO_2 Capture by Chemical-Looping Combustion. *Chem. Eng. Technol.* **2004**, *27*, 1318–1326, doi:10.1002/ceat.200402137.
59. Lyngfelt, A.; Leckner, B. A 1000 MWth Boiler for Chemical-Looping Combustion of Solid Fuels—Discussion of Design and Costs. *Appl. Energy* **2015**, *157*, 475–487, doi:10.1016/j.apenergy.2015.04.057.
60. Hetzer, J.; Kulik, R.; Rothenpieler, K.; Stückrath, K.; Weidenfeller, D.J. Design, Simulation and Practical Experience of the Largest Syngas Cooler in Operation for Coal Gasification. In Proceedings of the 8th International Freiberg Conference, Cologne, Germany, 12–16 June 2016.